HHS Public Access

Author manuscript

Nat Med. Author manuscript; available in PMC 2019 May 01.

Published in final edited form as:

Nat Med. 2018 May ; 24(4): 484–490. doi:10.1038/nm.4502.

Restorative Effects of Human Neural Stem Cell Grafts to the Primate Spinal Cord

Ephron S. Rosenzweig[1], **John H. Brock**[1,2], **Paul Lu**[1,2], **Hiromi Kumamaru**[1], **Ernesto A. Salegio**[3], **Ken Kadoya**[1,4], **Janet L. Weber**[1], **Justine J. Liang**[1], **Rod Moseanko**[3], **Stephanie Hawbecker**[3], **J. Russell Huie**[5], **Leif A. Havton**[6], **Yvette S. Nout-Lomas**[7], **Adam R. Ferguson**[5,8], **Michael S. Beattie**[5], **Jacqueline C. Bresnahan**[5], and **Mark H. Tuszynski**[1,2,*]

[1]Dept. of Neurosciences, University of California - San Diego, La Jolla, CA

[2]Veterans Administration Medical Center, La Jolla, CA

[3]California National Primate Research Center, University of California, Davis, CA

[4]Department of Orthopaedic Surgery, Hokkaido University, Sapporo, Japan

[5]Dept. of Neurosurgery, University of California, San Francisco, CA

[6]Dept. of Neurology, University of California, Los Angeles, CA

[7]College of Veterinary Medicine and Biomedical Sciences, Colorado State University, Fort Collins, CO

[8]Veterans Administration Medical Center, San Francisco, CA

Abstract

We grafted human spinal cord-derived neural progenitor cells (NPCs) into sites of cervical spinal cord injury in rhesus monkeys. Using 3-drug immunosuppression, grafts survived at least 9 months post-injury and expressed both neuronal and glial markers. Monkey axons regenerated into grafts and formed synapses. Hundreds of thousands of human axons extended out from grafts through monkey white matter and synapsed in distal gray matter. Grafts gradually matured over nine months, and improved forelimb function after a several month delay. These findings in a "pre-clinical trial" support translation to humans with the objective of reconstituting both a neuronal and glial milieu in the site of spinal cord injury.

Three decades of spinal cord injury (SCI) research have made it clear that abundant, long-distance regeneration of injured axons, which might improve function below a lesion site,

Correspondence to: Mark H. Tuszynski, Dept. Neurosciences, 0626, University of California, San Diego, La Jolla, CA 92093, 858-534-8857, 858-534-5220 (fax), mtuszynski@ucsd.edu.

AUTHOR CONTRIBUTIONS:

ESR, JHB, PL, EAS, KK, LAH, YSN-L, ARF, MSB, JCB, and MHT designed experiments.
ESR, JHB, PL, HK, EAS, KK, RM, SH, YSN-L, JCB, and MHT carried out experiments.
ESR, JHB, HK, EAS, JLW, JJL, JRH, LAH, ARF, and MHT analyzed data.
ESR and MHT wrote the manuscript.
ESR, JHB, PL, HK, EAS, KK, JLW, JJL, RM, SH, JRH, LAH, YSN-L, ARF, MSB, JCB, and MHT edited the manuscript.

COMPETING FINANCIAL INTERESTS:

The authors declare that they have no competing financial interests in this work.

remains elusive [e.g., 1]. Numerous extrinsic mechanisms contribute to failure of axonal regeneration after SCI, including an inhibitory extracellular matrix that develops around the site of injury [2,3], inhibitory myelin-associated proteins [4,5], and a lack of growth-promoting factors such as neurotrophins [6] in appropriate spatial and temporal gradients to promote growth.

Failure of neuron-intrinsic mechanisms also contributes to the lack of axonal regeneration in the adult CNS, and enhancing those intrinsic neuronal growth mechanisms overcomes extrinsic inhibitors [7,8]. Neurons derived from the developing spinal cord, for example, have active growth programs that support robust axon extension, and may be insensitive to inhibitors present in adult CNS [9–11]. This suggests an alternative approach to improving recovery after SCI: graft neural progenitor/stem cells into the injury site to form a neuronal relay circuit across the gap [9–15]. Such relay circuits are conceptually similar to those formed by propriospinal circuits after incomplete SCI [16]. To create such a circuit, a critical mass of grafted cells must: 1) survive and differentiate into neurons; 2) support growth of injured host axons into the graft; 3) accept synapses from these host-derived axons; 4) extend axons into the host spinal cord; and 5) form synapses on host neurons below the lesion (Fig. 1A). Building on this concept, we recently optimized methods for grafting neural stem cells to sites of SCI in rodents that improve electrophysiological and functional outcomes after even severe SCI [17–19]. Moreover, spinal cord re-transection immediately rostral to established grafts reverses electrophysiological and functional recovery, supporting the hypothesis that these implants form new neural relays across the lesion [17]. These findings support the possibility that neural stem cell grafting could promote neural repair after human SCI.

A non-human primate model of SCI can address numerous points related to clinical translation, including species differences in: 1) intrinsic stem cell biology, procurement and maturation, 2) CNS size and functional neuroanatomy, and 3) immune mechanisms [20–23]. Indeed, a number of experimental therapies showing efficacy in rodent models may be ineffective or impractical in primates [24], failing for numerous reasons that can include differences in intrinsic biology, small effect sizes, poor safety/tolerability, and lack of scalability of methods developed in rodents to humans [25]. Primate studies can be of great importance in addressing these issues prior to human clinical trials [24]. Indeed, recent reports support the paramount importance of validation of translational programs prior to human implementation [26], and proof of principle in a primate model is key on this path [24].

We now report successful engraftment of human spinal cord-derived multipotent neural progenitor cells into rhesus monkeys after SCI. Human neural progenitor cells extend up to hundreds of thousands of axons through degenerating white matter into the host spinal cord, forming reciprocal synaptic connections with host circuits. Grafts are safe and well-tolerated, and improve functional outcomes.

RESULTS

A total of nine adult male rhesus monkeys underwent implantation of human spinal cord-derived neural progenitors cells. Monkeys underwent right-sided C7 hemisection lesions, as previously described [27], two weeks prior to grafting. This two-week delay after injury is a clinically relevant time period in which humans might be expected to medically stabilize prior to undergoing neural stem cell therapy. On the day of grafting, the spinal cord lesion site was surgically re-exposed and scar tissue on the dorsal aspect of the spinal cord was incised (Fig. 1B,C). Viscous fluid containing cellular debris was released from the lesion site, and the open lesion cavity was microscopically visualized in its entirety and freed of internal adhesions, if present. A total of 20 million cells were then grafted into the lesion cavity using sterilized 100μl pipettors (Eppendorf, Hauppauge, NY) held freehand. Grafted cells consisted of GFP-expressing human multipotent neural progenitor cells isolated from an 8-week old human embryonic spinal cord, and maintained as a stable cell line (566RSC-UBQT line, a gift from NeuralStem Inc., Rockville, MD)[28–30]. Cells were shipped overnight from Maryland to the UC Davis primate research center, arriving on the day of implantation. Immediately prior to grafting, cells were suspended in a growth factor cocktail and fibrin/thrombin matrix, as employed in rodent experiments (see Methods; [17,18]).

Development of Grafting Methods

Highlighting the vital importance of large animal models in translational studies, our initial efforts to transplant human neural progenitor cells into four monkeys failed to support graft survival, despite use of methods that were successful in rodents. First, we found that cerebrospinal fluid (CSF) rapidly filled the lesion cavity and washed away grafted cells, despite the use of a rapidly gelling fibrin/thrombin matrix. Thus, the first two subjects had no surviving cells. Employing a historical method for draining CSF in humans, in all subsequent monkeys we tilted the operative table to a 30° angle immediately prior to grafting to drain CSF from the cervical spinal cord; this action provides a 15-minute period in which the lesion cavity is free of CSF. We also increased the fibrin and thrombin concentration in the grafting mixture to generate rapid gelling (within 3 seconds). In the next two subjects, these measures resulted in filling of the lesion site with cells at the conclusion of the grafting session. However, when examined two months later, while some graft cell survival was evident, cells failed to fill the entire lesion cavity. Monkeys up to this point had been immunosuppressed with low initial doses of mycophenolate mofetil and tacrolimus (see Methods). Beginning with Subject 5 we adopted a more robust clinical organ transplantation immunosuppressive regimen, with higher initial doses of mycophenolate mofetil and tacrolimus, and more frequent (2–3x/wk) monitoring of immunosuppressant drug levels until therapeutic doses were well established. Using these measures, graft survival and fill of the lesion site was achieved in the five subsequent subjects (Fig. 1D; Suppl. Fig. 1).

Human Stem Cell Grafts Survive and Extend Large Numbers of Axons Over Long Distances in the Lesioned Primate Spinal Cord

Using these optimized grafting methods in 5 subsequent subjects, NPCs survived in C7 hemisection lesion cavities from two through nine months (Fig. 1D; Suppl. Fig. 1). Grafts

occupied the majority of the lesion cavity in all subjects and integrated well with the host spinal cord. Neuronal markers were readily detectable in grafts at all time points, from two to nine months after grafting (Fig. 1). The early neuronal marker doublecortin was predominant two-months post-grafting and declined but remained detectable after nine months (Fig. 1G). The more mature neuronal marker NeuN was also detected two months post-grafting (Fig. 1E,F) and continued to be expressed over time. The density of cells in the graft was highest two months post-implantation (400,000 cells/mm^3) and steadily dropped 63% to 150,000 cells/mm^3 nine months post-grafting (R^2=0.93, P=0.007; Fig. 2A and Table 1). In contrast, cell size steadily increased over the same time period (R^2=0.82, P=0.03; Fig. 2B and Table 1). Grafts expressed the early astrocyte filamentous marker vimentin at the earliest time point examined, two months post-implantation (Fig. 1H). Glial fibrillary acidic protein (GFAP), a marker of more mature astrocytes, was not detectably co-localized with GFP until 5 months post-grafting (Fig. 1I), suggesting a prolonged period of astrocyte maturation as well. Of the three cardinal cell types of the CNS, the relative proportions of cells expressing neuronal (NeuN), astrocyte (Sox9), and oligodendrocyte (Olig2) markers was 57 ± 10%, 26 ± 5%, and 17 ± 7%, respectively (Fig. 1E, J, K); these proportions were calculated from analysis of a mean of 766 ± 100 individual cells per subject. Astrocyte identity was confirmed in 80% of $Sox9^+$ cells by GFAP co-labeling in Subjects 8 & 9 [31,32]. Oligodendrocyte lineage was confirmed in all $Olig2^+$ cells by a lack of colabeling with Isl1/2 (ESR, JHB, JLW, HK, MHT, data not shown); the lack of graft-derived cell migration (see below) suggests that these cells are likely immature non-myelinating oligodendrocytes. No graft-derived cells expressed Opalin, a marker of mature myelinating oligodendrocytes [33](Suppl. Fig. 2), indicating that mature oligodendrocytes were not yet present in grafts. The proportion of dividing cells in grafts, as assessed by Ki-67 labeling (Fig. 1L), was low at all time points (mean 1.5 ± 0.5%); it was 0.7% at 9 mos post-grafting. Teratomas or tumors were not detected in any subject.

Notably, human axons emerged from grafts in extraordinary numbers and over long distances. Up to 150,000 graft-derived axons were present 2 mm caudal to the lesion, 2–9 months post-grafting (Figs. 2 and 3, Table 1, and Suppl. Fig. 1), and axons reached distances up to 50 mm from the graft (Suppl. Fig. 3). Axons emerged rostrally in similar numbers and over similar distances (Suppl. Fig. 3). Axons extended into white matter tracts that were directly abutted against grafts, and appeared to maintain growth within these same white matter fascicles to points distant from the graft (Suppl. Fig. 4); this observation suggests that axons may continue to extend through the white matter tracts that they first encounter upon emerging from grafts in the lesion site. Furthermore, the fact that human axons extended linearly through host white matter (Fig. 3 and Suppl. Figs. 1,3,4), suggests that myelin does not inhibit the growth of these developmental-stage human axons, a finding consistent with observations in non-primate models [9–12,17–19].

Emerging axons expressed βIII tubulin, a marker of both immature and mature axons, light-chain neurofilament (NF70), a marker of both immature and mature small-diameter axons, and unphosphorylated heavy-chain neurofilament (SMI32), another immature axon marker (Suppl. Fig. 5). Graft-derived axons did not express phosphorylated heavy-chain neurofilament (NF200; Fig. 4F inset), a marker expressed in many mature human axons (Suppl. Fig. 6). Thus, axons were not fully mature even 9 months post-grafting, consistent

with neuronal size measures and delayed expression of GFAP as noted above, and consistent with delayed maturation of other human neural stem cells in rodent SCI [34]. Synapse formation was readily detected between graft-derived axons and host neurons in the spinal cord caudal to the lesion site, reflected both by apposition of postsynaptic homer1 with presynaptic GFP and synaptophysin, and by ultrastructural analysis (Fig. 3, Suppl. Figs. 7–8). Extending human axons frequently converged onto host motor neurons, wrapping motor neuronal somata with dozens of appositions that co-localized with the synaptic marker synaptophysin (Fig. 3F,G). Ultrastructurally, all observed graft-host synapses had clear, spheroid vesicles in the pre-synaptic bouton, and synaptic specializations in the plane of sectioning were characteristically asymmetric, features indicative of an excitatory phenotype (Fig. 3H–J, Suppl. Fig. 8), as expected of long-projecting axons [35]. Consistent with the apparent immature state of graft-derived axons, we did not detect myelination of graft-derived axons caudal to the lesion site that were up to 1 μm diameter, through 9 months post-grafting (Suppl. Fig. 6). In contrast, axons emerging from more rapidly maturing rodent neural progenitor cells grafted into rats are readily myelinated by two months post-implantation [17].

Host Axons Regenerate into Human Neural Stem Cell Grafts

In theory, human neural stem cell implantation into a lesion cavity aims to re-establish a neuronal relay across a site of SCI. For this to occur, host axons must regenerate *into* neural stem cell grafts, and neural stem cell implants must extend axons out of grafts and into the host spinal cord. To assess whether host axons regenerate into human neural progenitor cell grafts, we performed immunolabeling for NF200 (which is not expressed by grafted neurons; Fig. 4F inset) and serotonergic motor axons, and performed anterograde tracing of the corticospinal system using intracortical injections of biotinylated dextran amine (BDA). Notably, grafts were extensively and densely penetrated by host NF-200 labeled axons beginning two months post-grafting and persisting through nine months (Fig. 4E,F). Many NF200-labeled axons originate from intraspinal neuronal circuits. Serotonergic axons, critical for modulation of locomotion, muscle tone and pain responses [36,37], also penetrated grafts (Fig. 4C,D).

The corticospinal projection is the most important neuronal system for voluntary movement in humans, and its regeneration is likely to be important for enhancing voluntary motor movement after SCI in humans. Yet this system is the most refractory axonal system from which to elicit axonal regeneration into a lesion site [1](Suppl. Fig. 9). Recently we reported in rodent models that grafts of neural stem cells driven to a spinal cord identity support regeneration of corticospinal axons [19]. We now report for the first time the regeneration of primate corticospinal axons into human NPC grafts (Fig. 4A,B). Corticospinal axons readily crossed the host/graft interface to penetrate distances up to 500μm into the graft (Fig. 4B).

Functional Outcomes

Animals were scored in an open field task that samples over 25 features of motor function [38–40], including several subscales that score object manipulation, climbing and overground locomotion as monkeys engage in naturalistic behaviors in a large testing enclosure [38–40] (Suppl. Fig. 10). Animals receive points for function in each behavioral

category with a composite score representing an overall assessment of neurological function. The primate C7 lesion model was designed to assess potential therapies for improving distal forelimb function, since neural circuitry for hand control is located in the C7-T1 spinal levels that range from 1mm to 20mm below the lesion, and axons extending from a neural stem cell graft reach these segments (Figs. 2,3). Function among monkeys with non-surviving grafts (Subjects 1–4) exhibited stability or only partial spontaneous improvement up to 4–8 weeks post-injury, but was then stable without subsequent overall improvement (Suppl. Figs. 10,11), a pattern consistent with previous studies in lesion-only control subjects [27,38] (Suppl. Fig. 11). In contrast, among monkeys with surviving grafts, the initial 4–8 week post-lesion period of functional loss or partial spontaneous improvement was followed by a second period of subsequent improvement after 10 weeks (Suppl. Fig. 10). Object manipulation recovered to >25% success in 4 of 5 monkeys with grafts, but in only 1 of 4 monkeys without grafts. Moreover, peak right hand object manipulation performance was greater in monkeys with grafts ($P<0.01$, Wald Chi-square; Suppl. Fig. 10). In contrast, the climbing score, which measures both forelimb and hindlimb use, did not differ significantly between monkeys with and without surviving grafts ($p=0.19$; Wald Chi-square; Suppl. Fig. 10). Unlike object manipulation, locomotor recovery is fairly extensive after C7 hemisection in monkeys, as in humans [41], and values on this subscale differed between surviving and non-surviving graft groups by only 12%, a modest amount that was nonetheless significant ($P=0.05$, Wald Chi-square; Suppl. Fig. 10). On an *overall* measure of motor function that combines all measures, monkeys with surviving grafts exhibited a significant degree of improvement in peak performance compared to monkeys without surviving grafts ($P=0.02$, Wald Chi-square; Suppl. Fig. 10).

A composite behavioral score was also generated using non-linear principal components analysis (PCA), on functional outcome data. This demonstrated a significant difference in multidimensional recovery curves between monkeys with surviving grafts compared to non-surviving grafts, employing a last observation-carried forward analysis and linear mixed model testing ($P<0.05$; Suppl. Figs. 10,12). These results are interpreted with caution because the study did not contain a lesioned control group in which no attempt to graft was made, and because monkeys with poor graft survival did not survive as long as monkeys with surviving grafts (Subjects 1–4 were enrolled earlier in the study and were pre-planned for early termination to assess graft survival). However, three points support the probability that these statistically significant improvements in function in monkeys with surviving grafts reflect true recovery: a) control lesioned animals from previous [27,38] and recent (Suppl. Fig. 11) studies do not exhibit late functional recovery of the type observed in successfully grafted monkeys; b) one monkey without graft survival in the present study that was perfused after 21 weeks did not show late improvement (Suppl. Fig. 10B); and c) improvements were proportionately greater on measures of forelimb than hindlimb function in successfully grafted subjects, a pattern consistent with dense penetration of graft-derived axons into cervical spinal cord segments (Fig. 3).

Cells Do Not Migrate from the Lesion Site or form Ectopic Colonies

Previous studies have reported long-distance migration of human neural stem cells implanted into rodent models; this migration has consisted nearly entirely of glia [42]. In

this study we did not observe migration of human neurons or glia more than 100 μm from the lesion site (c.f. Fig. 3, Suppl. Figs. 1,3). This result is consistent with graft-derived Olig2$^+$ cells representing immature oligodendrocytes, rather than migratory oligodendrocyte progenitor cells [43]. Also in rodent models, ectopic deposits of grafted neural stem cells have been observed along the spinal cord central canal and on the surface of the spinal cord [44,45]. In the present study, we did not observe migration of implanted human neural progenitor cells in the central canal, ventricles or brain. In one subject, a single GFP-expressing NPC colony was present on the spinal cord surface directly at the site of engraftment, but not at more distal sites.

Lesions in all nine animals were very similar in extent (Suppl. Fig. 13). Grafts were well vascularized, as revealed by both Nissl stains and collagen immunolabeling (Suppl. Fig. 14). Mild perivascular cellular infiltrates consisting of CD8+ T-cells were present in fully immunosuppressed animals, suggesting an ongoing, low-grade immune response that continued nine months post-grafting (Suppl. Fig. 14).

Visualization of Grafts by MRI

We performed high-resolution 3D T1 and T2 weighted isotropic MRI scans on a 3 Tesla Siemens clinical MR scanner in monkeys sedated with ketamine (5mg/kg) after grafting to determine whether fill of the lesion site could be detected in the living subject. Findings were compared to anatomical analyses (Fig. 1, Suppl. Fig 1). Monkeys lacking surviving grafts exhibited low signal on T1-weighted imaging and high signal on T2-weighted imaging in the lesion site, whereas monkeys with surviving grafts exhibited opposing results (Suppl. Fig. 15).

DISCUSSION

Four important observations arise from this study. First, human neural stem cells can be successfully engrafted to fill the large lesion cavity of a non-human primate spinal cord, using methods that are unique to the primate model. These methods include an increased concentration of fibrinogen and thrombin in the grafting mixture, and intra-operative drainage of CSF to create a dry grafting cavity. Second, human grafts exhibit a prolonged time period of maturation. Although grafts continued to mature over the nine-month period of this study, functional effects of grafts may have been evident by 3–4 months post-grafting, when axons have already extended 50 mm into the host. Immature axons and synapses conduct action potentials and are capable of influencing signal processing in the hippocampus [46,47]; similarly active immature graft-derived axons could account for the functional benefits observed herein. Third, unprecedented numbers of new human axons are capable of extending out from the lesion site and into the spinal cord surrounding the site of injury: up to 150,000 axons extend from the lesion on one side of the spinal cord, a substantial mass of new circuitry that represents a potential mechanism for influencing functional outcomes. To date, with observations of functional outcomes through nine months, partial functional recovery occurs. It is possible that more prolonged observation periods could result in yet greater recovery. Fourth, we describe for the first time the

regeneration of corticospinal axons, essential for voluntary movement in humans, into a lesion site in the primate.

Highlighting a critical feature of scaling up to larger animal models, we found that grafting methods that were effective in rodent models did *not* enable graft survival in non-human primates. Following several modifications to the rodent grafting technique, including modifications to the grafting matrix, physical measures (operative table tilt to drain CSF) and more extensive immunosuppression, successful engraftment was achieved. Had we or others attempted human translation without large animal testing, there would have been a substantial risk of clinical trial failure not as a result of failure of the biological potential of neural stem cells, but as a simple result of graft loss. It is important that invasive cellular translational studies avoid these pitfalls and utilize larger animal models when possible [24,25].

A key limiting factor in the translational relevance of previous repair efforts in SCI has been limited regeneration of corticospinal axons [48,49]. While enhanced sprouting of host axons in spared host gray matter after SCI by manipulation of phosphatase and tensin homolog (PTEN) and suppressor of cytokine signaling 3 (SOCS3) is impressive [50,51], these genetic manipulations primarily promoted corticospinal growth in spared regions of the host spinal cord, rather than regeneration into spinal cord lesion sites themselves. Yet the majority of human injuries are clinically complete, and it is unclear whether targeting the relatively low number of corticospinal axons in small regions of spared host matter will be useful [52]. Thus, achieving corticospinal regeneration into a lesion site is likely to be important in translational human therapies for severe injury [53]. We recently reported that spinal cord replacement with homologous spinal cord neural anlage supports corticospinal axon regeneration into lesion sites in rodents, and enhances forelimb reaching function [19]. In the present study, *primate* corticospinal axons also regenerated into human neural stem cells grafted to lesion sites. Given the critical role of corticospinal systems in human fine motor control, their regeneration represents an important milestone in translational relevance in a primate model. Corticospinal axons regenerated ~0.5mm into grafts. In future studies we will determine whether greater distances and densities of corticospinal penetration might be achieved using drugs that enhance the endogenous growth state of host neurons, such as transient treatment with pharmacological PTEN inhibitors [50,54,55].

Grafts exhibited evidence of continuing maturation over time. Astrocytes first expressed the mature marker GFAP five months post-grafting, and neurons continued to exhibit increasing somal size over nine months. Numbers of grafted neurons fell by approximately 50% at longer time points, consistent with patterns observed in normal neural development [56–58]. It is possible that graft neurons that failed to form stable synapses were selectively eliminated [59]. It is important that future human clinical trials take into consideration the possibility that grafts will mature gradually, with potentially late effects on functional outcomes.

Finally, a major barrier to achieving adult axon regeneration has been the axon-growth-inhibitory nature of adult myelin [4,5]. Here we show that axons emerging from human neural stem cells extend abundant axons through white matter, overcoming a major limiting

factor in the regeneration field. In parallel, *host* adult axons regenerated into the myelin-free stem cell environment. Accordingly, neural stem cell therapy represents a means of circumventing one of the major challenges to axon regeneration in the adult CNS.

ONLINE METHODS

Subjects—We studied a total of nine naïve male rhesus macaques (*Macaca mulatta*), aged 6–10 years. Post-hoc anatomical analyses separated the subjects into two groups, according to graft survival (N=4 without grafts; N=5 with grafts). Our previous work in this model of SCI has demonstrated sufficiently low variability to achieve statistical significance with groups of this size [27]. All surgical and experimental procedures adhered to the principles outlined by American Association for the Accreditation of Laboratory Animal Care and were approved by the Institutional Animal Care and Use Committee (IACUC). Subjects were housed and surgeries performed at the California National Primate Research Center (Davis, CA). Subsequent tissue processing and analysis was performed at the Center for Neural Repair (University of California, San Diego; La Jolla, CA). Additional reporting information is available in the Life Sciences Reporting Summary, published alongside this work.

Lesion surgery—Animals were sedated with 1 mg/kg ketamine intramuscularly and anesthetized with 1.5–2.5% isoflurane. The caudal half of the C5 dorsal lamina and the entire C6 dorsal lamina were removed. The dura was slit longitudinally along the midline and retracted gently. A surgical micro-knife was mounted on a stereotaxic arm positioned at the spinal midline midway between the C5 and C6 dorsal laminae. This rostrocaudal position corresponds to the C7 spinal cord segment. The stereotaxic manipulator was used to lower the blade through the entire dorsoventral extent of the spinal cord without severing the ventral artery. This initial cut established the medial position of the lesion. The lesion was then completed using microscissors under microscopic observation by the surgeon to ensure lesion completeness laterally and ventrally. Animals retained bowel, bladder, and autonomic function after SCI. Lesion reconstructions are shown in Suppl. Fig. 13.

Immunosuppression—All grafted subjects received a triple immunosuppressive regimen consisting of mycophenolate mofetil (MMF; CellSept), tacrolimus (FK-506; ProGraf), and prednisone. These drugs were begun one day prior to grafting and were administered orally or through a nasogastric tube. In all subjects, the initial dose of prednisone was 2 mg/kg/day and was reduced to 1 mg/kg/day on the second day after transplantation. In subjects 1–4, initial dosage of MMF was 50 mg/kg/day, initial dosage of FK-506 was 0.3 mg/kg/day, both drugs split across 2 doses (AM/PM). Due to poor graft survival in subjects 1–4, initial dosages of MMF and FK-506 were increased to 100 mg/kg/day and 1 mg/kg/day, respectively. Blood trough levels of MMF (target range 3–6 μg/mL) and FK-506 (target range 4–10 ng/mL) were assessed 1–3 times/wk to adjust dosages. Immunosuppression continued until date of sacrifice.

Grafting—Two weeks after the C7 right lateral hemisection, we grafted twenty million GFP-expressing human neural progenitor cells into the lesion site. This karyotypically stable

cell line (566RSC-UBQT) was derived from the lower cervical/upper thoracic spinal cord of an 8 week old fetus, donated in accordance with NIH and FDA guidelines [28]. As previously reported [29,30], the vast majority (94%) of these cells express nestin and are uncommitted to neuronal or glial lineage prior to transplantation. These cells are maintained, authenticated, and tested for mycoplasma by NeuralStem, Inc. hNPCs were shipped by overnight delivery at 4°C while suspended at 20,000 cells/μl in a proprietary hibernation medium. Subjects were sedated and anesthetized as described above, and the lesion site was re-exposed. Hibernation media were removed, then hNPCs were suspended at 200,000 cells/μl in a two-part fibrin matrix (human fibrinogen, Sigma, F3879, 100 mg/mL; human thrombin, Sigma, T7009, 100 U/mL) containing a cocktail of growth factors: BDNF (50 μg/mL, Peprotech, 452-02), neurotrophin-3 (NT-3; 50 μg/mL, Peprotech, 450-03), glial-cell-line-derived neurotrophic factor (GDNF; 10 μg/mL, Sigma, G1401), epidermal growth factor (EGF; 10 μg/mL, Sigma, E1257), basic fibroblast growth factor (bFGF; 10 μg/mL, Sigma, F0291), acidic fibroblast growth factor (aFGF; 10 μg/mL, Sigma, F5542), hepatocyte growth factor (HGF; 10 μg/mL, Sigma, H9661), insulin-like growth factor 1 (IGF-1; 10 μg/mL, Sigma, I8779), platelet-derived growth factor (PDGF-AA; 10 μg/mL, Peprotech, 100-13A), vascular endothelial growth factor (VEGF; 10 μg/mL, Peprotech, 100-20), and a calpain inhibitor (MDL28170, 50 μM, Sigma, M6690). In subjects 3–9, immediately prior to the placement of cells into the lesion site, the surgical table was tilted approximately 30 degrees (head upward). This temporarily drains cerebrospinal fluid away from the lesion site, providing 5–15 minutes for surgeons to place the cells and for the liquid components of the fibrin matrix to form a gel, holding the NPCs in the lesion site. After the gel had formed, the dura, muscles and fascia, and skin were sutured closed in layers.

Corticospinal tracing—Corticospinal tract (CST) axons were traced in Subject 9 to assess regeneration into the graft. As previously described [20], six weeks prior to sacrifice, the subject was anesthetized and a craniotomy was performed to expose the left motor cortex. 300 nl of the anterograde neuronal tracer biotinylated dextran amine (BDA; 10,000 MW, 10% in water, Thermo Fisher) was injected at each of 127 sites (59 different surface locations). These sites included motor cortex innervating the hand, arm, trunk, leg, and foot.

Tissue processing—Subjects were sacrificed 2–9 months after receiving hNPC grafts. Subjects were deeply anesthetized and transcardially perfused with a 4% solution of paraformaldehyde, and the spinal cord was dissected out of the spinal column. Spinal cord dura was removed, and the spinal cord was cut in the transverse plane into 1- or 1.5-cm-long blocks as detailed previously [27]. The block containing the lesion was cut into 30-μm-thick horizontal sections using a freezing microtome. Additional blocks of tissue were cut into 40-μm-thick transverse sections. In Subject 9, the tissue blocks immediately rostral and caudal to the lesion block were first partially cut (six 50-μm-thick transverse sections) using a vibratome, a method more compatible with electron microscopy. The vibratome-cut sections were immediately immunolabeled for green fluorescent protein (see below), while the remaining tissue in those blocks was cut on a microtome in the same fashion as the other spinal cords. Tissue sections were stored at −20 °C in TCS cryoprotectant (25% glycerin (v/v), 30% ethylene glycol (v/v) in 0.5-M phosphate buffer).

Fluorescent immunolabeling—Transverse sections were pre-treated with 50% methanol for 20 min at 22–24°C, washed in tris-buffered saline (TBS) and blocked for 1 hr in TBS containing 5% normal donkey serum and 0.25% Triton X-100. Sections were incubated in primary antibodies against GFP (rabbit, Thermo Fisher, 1:1500); GFAP (chicken, Genetex, 1:1500, to label astrocytes); NeuN (mouse, Millipore, 1:1000, to label mature neurons); βIIITubulin (mouse, Promega, 1:1000, to label immature and mature neurons); neurofilament light-chain (NF70, mouse, Millipore, 1:300, to label immature axons); neurofilament unphosphorylated heavy-chain (SMI32, mouse, Covance, 1:2000); neurofilament phosphorylated heavy-chain (NF200, mouse, Millipore, 1:500); Ki-67 (rabbit, Abcam, 1:250, to label dividing cells); Olig2 (rabbit, IBL, 1:200, to label oligodendrocytes and MN precursors); Opalin (mouse, Santa Cruz Biotechnology, 1:200, to label myelinating oligodendrocytes); Sox9 (goat, R&D Systems, 1:1000, to label astrocytes and ependymal cells); and Homer1 (rabbit, Synaptic Systems, 1:1000, to label post-synaptic densities). BDA was detected with Alexa-Fluor 594- or 568-conjugated streptavidin (Thermo Fisher, 1:1000). Sections were washed with TBS and then incubated in Alexa-Fluor 488- or 594-conjugated anti-goat or anti-donkey secondary antibodies (Thermo Fisher, 1:500) for 1 hour and 4′,6-diamidino-2-phenylindole (DAPI, Sigma, 0.5ug/ul, to label nuclei) for 5 min. Sections were washed with TBS, mounted on slides, and coverslipped with Mowiol mounting medium (http://cshprotocols.cshlp.org/content/2006/1/pdb.rec10255). All antibodies were used previously in monkeys and/or on the 566RSC-UBQT cell line [17,27,28].

Electron microscopy—Some tissue sections from Subject 9 were analyzed with a combination of immunolabeling (for GFP) and electron microscopy (to identify synaptic structures). Sections were post-fixed for 1 hr in 0.1% glutaraldehyde in 0.1 M phosphate buffer (PB), then endogenous peroxidase activity was quenched in 0.6% H_2O_2 in TBS for 30 min. Sections were permeabilized in 50% ethanol in TBS for 30 min, incubated in 1% sodium borohydride in TBS for 30 min, and blocked in 5% horse serum and 0.025% Triton X-100 in TBS for 1 hr. Sections were incubated for 3 nights in primary antibody (rabbit anti-GFP, Thermo Fisher #A6455, 1:3000 in blocking buffer). Sections were then incubated for 1 hr in Vector Impress Poly-HRP secondary antibody (Vector #MP-7401, 1:1 in TBS). Finally, a visible reaction product was developed in 0.05% diaminobenzidene, 0.04% nickel chloride, 0.012% H^20^2 in TBS for approximately 4 minutes. Wet sections were next examined by light microscopy, and portions containing visible reaction products within the spinal cord grey matter were trimmed and processed for ultrastructural studies. The trimmed sections were first immersed in a 1% osmium tetroxide solution (Ted Pella, Inc.), dehydrated in a graded series of ethanol, and immersed in 100% propylene oxide. Sections were next embedded in an epoxy resin using the Eponate 12 kit with DMP-30 as an accelerator (Ted Pella, Inc. #18010). Ultrathin sections were cut at 60–70 nm section thickness using an RMC Products PowerTome Ultramicrotome (Boeckeler Instruments), and the ultrathin sections were collected on formvar-coated one-hole copper grids. The sections were contrasted with uranyl acetate and lead citrate. The ultrathin sections were finally examined in a JEOL 100 CX transmission electron microscope. Neuronal processes containing electron dense reaction products were photographed at 7,200X, and images were captured on electron microscope film (Electron Microscopy Sciences).

Image acquisition—Epifluorescent images were captured using an Optronics Microfire A/R digital camera (www.optronics.com) or using a Keyence BZ-X710 All-in-one microscope and camera. Confocal images were captured with an Olympus Fluoview FV1000 confocal microscope (www.olympusamerica.com) set for sequential scanning. For publication, images were processed uniformly for optimal brightness and contrast using Adobe Photoshop CS5 (Adobe Systems, San Jose, CA). Images intended for quantification (see below) were not modified in this fashion. Composites of multiple focal planes were constructed either in Adobe Photoshop CS5 or ImageJ 1.48v (Wayne Rasband, National Institutes of Health, rsb.info.nih.gov/ij/).

Quantification of graft volume, neural cell density, and axon number—Graft-derived cells were quantified in confocal image stacks by counting individual cells labeled for GFP and NeuN within a fixed rectangular region of interest (ROI) drawn with ImageJ. All cells within the ROI were counted and area was quantified. For each animal, 5–14 image stacks (spread in a grid across the graft) were quantified (a mean of 766 ± 100 individual cells per subject). Cell density was estimated by dividing the number of cells by ROI volume. Additional estimates of the proportion of cells in the graft co-expressing NeuN, Olig2, Sox9, or Ki-67 were made under epifluorescent illumination using StereoInvestigator (MicroBrightfield, http://www.mbfbioscience.com). Graft area was measured in horizontal tissue sections (1:12 series; a mean of 14.4 ± 0.9 sections per animal) under epifluorescent illumination using StereoInvestigator. Graft volume was estimated as: (summed area across all sections) x (avg. section thickness) x (inverse of the sampling frequency).

Total graft-derived cell counts were estimated by multiplying the cell density by the graft volume. The number of GFP-labeled axons was quantified under epifluorescent illumination using StereoInvestigator (MicroBrightfield, http://www.mbfbioscience.com). In horizontal tissue sections (1:12 series), using a 4x objective, a transverse line was drawn 2 mm caudal to the edge of the graft. Using a 60x objective, axons that intersected the line were marked and counted, and total axon number per subject was estimated by multiplying the axon count by the inverse of the sampling frequency.

Functional testing—Functional recovery was evaluated weekly throughout the study in an open-field task previously developed by our group to assess general motor function and overground locomotion, climbing and object manipulation [38–40]. Behavioral assessments in this open field were typically performed live with two observers: one videotaping the session (RM or SH), and one recording behavioral observations on the scoring sheet (ES or JCB). Alternatively, sessions were scored directly from the video; the videos were also used to confirm live scoring results. Inter-rater reliability was evaluated periodically and high levels of agreement were obtained (ES & JCB). All assessments were performed without knowledge of group inclusion as the observers had no way of knowing which animals had surviving transplants. Monkeys entered an open field testing enclosure (7ft × 10ft × 6 ft high), and had access to four ascending perches, to reach a food reward placed inside a Kong (a hollow rubber toy filled with raisins, apple pieces, peanuts, dry fruit, etc; Kong Co., Golden CO) positioned on the highest perch. Locomotor activity was evaluated while the animals traversed the perches as well as on the floor of the open cage. Climbing was

assessed during retrieval of similar food objects placed in cups hanging at various heights (1.5, 2.7. 3.5, 4.3 and 4.7ft) along the front of the cage. Object manipulation was assessed during manipulation of the Kong toy and during the consumption of a large food item to encourage bimanual manipulation (e.g. an apple or orange; see Suppl. Fig. 10). A modified 72-point scale was used and assigned points for behavioral function. The object manipulation subscale had 22 points and was used to assess forelimb function while manipulating objects and scored posture, object support on and off the ground, joint and finger movements, digit 1 opposition and pincer grasp. We compared the level of functional performance of monkeys with surviving grafts (N=5) and non-surviving grafts (N=4). Because groups were established after sacrifice, experimenters were blind to group membership. Although monkeys survived for differing lengths of time after grafting, the performance of all animals reached an asymptote during their survival period (Suppl. Fig. 10), as assessed by modified moving averages. Accordingly, we calculated the maximal score for each monkey during the period of asymptotic function (see Suppl. Figs. 10–12).

Statistical analysis and reproducibility—All immunohistochemical reactions were performed at least twice with similar results. Graft cell densities, sizes, and axon counts were analyzed with Matlab 2010b (MathWorks). The Corrcoef function was used to calculate the correlation (R^2) of these variables with survival time and the p-values of those correlations. Functional data were analyzed by applied biostatisticians (JRH; ARF) who were blinded to experimental conditions. Non-parametric tests on single (univariate) outcome measures were executed using generalized linear modeling (Gzlm) and significance assessed using the Wald Chi-square test. To assess the multivariate effect of behavioral outcome measures, we integrated these data using a modern data-driven analytics approach where a combined behavioral endpoint was derived by a multidimensional pattern detector (non-linear principal component analysis; NL-PCA), in an unsupervised manner, blind to experimental condition. Our analytical workflow involved two distinct stages of statistical analysis (Suppl. Fig. 12): Stage 1- multidimensional endpoint description using PCA, and validation of PC loading patterns; and Stage 2- hypothesis testing using validated multidimensional pattern (PC1) as the primary combinatorial endpoint. Stage 1 pattern detection was assessed using multidimensional endpoint variable integration into PC1, followed by examination of variance explained and PC loadings for statistical and face-validation respectively. Once that single, PCA-weight combined endpoint axis (PC1) was deemed reproducible and valid, we applied the PC weights to derive the unique PC score of each animal at each timepoint and rigorously validated using previously established statistical decision rules [60–63]. The PC scores were then plotted over time, and if an animal's recovery time did not reach 21 weeks, the last observed PC score for that animal was carried forward to 21 weeks using techniques consistent with best practices from the clinical literature [64]. Only after PC scores were mathematically derived for each subject and time point (Suppl. Fig. 12A–C) did we move to the Stage 2 hypothesis testing (Suppl. Fig. 12D–E). Hypothesis testing used PC scores as the primary endpoint to assess impact of graft condition on behavioral outcome. A linear mixed model (LMM; IBM SPSS 'Mixed' subcommand) was then applied to assess group differences in PC1 scores over time. This variance components approach is robust against missing data and independence violations that would otherwise undermine the validity of repeated measures ANOVA in this context.

Prior work from our group and others have demonstrated that PCA is robust and stable when used in this context (even with low N)[27,41], as long as the variance explained by PC1 is high and the communalities are high. These statistical features indicate that the combined information provided by the optimally-weighted combination of variables (PC1) is greater than the sum of the raw endpoint variables, independent of sample size [62]. The statistical analysis plan was carried out by the project's independent statistical analysis core (blinded to treatment until the final analysis step). The goal was to maximize information gain in the most transparent and statistically appropriate manner given the costs and the desire to limit subject numbers in primate studies [65]. All analyses were carried out in SPSS v.23 (IBM). PC loadings were considered significant at |0.4|. Significance for Gzlm and LMM was assessed at $p < 0.05$.

DATA AVAILABILITY

The data that support the findings of this study are available from the corresponding author upon reasonable request.

Supplementary Material

Refer to Web version on PubMed Central for supplementary material.

Acknowledgments

Human 566RSC-UBQT neural stem cells were a gift from NeuralStem, Inc. This work was supported by the NIH (R01 NS042291, MHT; R01 NS104442, MHT), the Veterans Administration (Gordon Mansfield Spinal Cord Injury Collaborative Consortium, RR&D B7332R, MHT; RR&D RX001045, JHB), the Department of Defense (W81XWH-12-1-0592, ESR), the Craig H. Neilsen Foundation (MHT), the Bernard and Anne Spitzer Charitable Trust (MHT), and the Dr. Miriam and Sheldon G. Adelson Medical Research Foundation (MHT).

References

1. Blesch A, Tuszynski MH. Spinal cord injury: plasticity, regeneration and the challenge of translational drug development. Trends Neurosci. 2009; 32:41–7. [PubMed: 18977039]
2. Fawcett JW. Overcoming inhibition in the damaged spinal cord. J Neurotrauma. 2006; 23:371–83. [PubMed: 16629623]
3. Fitch MT, Silver J. CNS injury, glial scars, and inflammation: Inhibitory extracellular matrices and regeneration failure. Exp Neurol. 2008; 209:294–301. [PubMed: 17617407]
4. He Z, Koprivica V. The Nogo signaling pathway for regeneration block. Annu Rev Neurosci. 2004; 27:341–68. [PubMed: 15217336]
5. Schwab ME. Nogo and axon regeneration. Curr Opin Neurobiol. 2004; 14:118–24. [PubMed: 15018947]
6. Lu P, Tuszynski MH. Growth factors and combinatorial therapies for CNS regeneration. Exp Neurol. 2008; 209:313–20. [PubMed: 17927983]
7. Filbin MT. Recapitulate development to promote axonal regeneration: good or bad approach? Philos. Trans R Soc Lond B Biol Sci. 2006; 361:1565–74.
8. Kadoya K, Tsukada S, Lu P, Coppola G, Geschwind D, Filbin MT, Blesch A, Tuszynski MH. Combined intrinsic and extrinsic neuronal mechanisms facilitate bridging axonal regeneration one year after spinal cord injury. Neuron. 2009; 64:165–72. [PubMed: 19874785]
9. Jakeman LB, Reier PJ. Axonal projections between fetal spinal cord transplants and the adult rat spinal cord: a neuroanatomical tracing study of local interactions. J Comp Neurol. 1991; 307:311–34. [PubMed: 1713233]

10. Reier PJ, Stokes BT, Thompson FJ, Anderson DK. Fetal cell grafts into resection and contusion/compression injuries of the rat and cat spinal cord. Exp Neurol. 1992; 115:177–88. [PubMed: 1370221]
11. Wictorin K, Björklund A. Axon outgrowth from grafts of human embryonic spinal cord in the lesioned adult rat spinal cord. Neuroreport. 1992; 3:1045–8. [PubMed: 1493215]
12. Coumans JV, Lin TT, Dai HN, MacArthur L, McAtee M, Nash C, Bregman BS. Axonal regeneration and functional recovery after complete spinal cord transection in rats by delayed treatment with transplants and neurotrophins. J Neurosci. 2001; 21:9334–44. [PubMed: 11717367]
13. Cummings BJ, Uchida N, Tamaki SJ, Salazar DL, Hooshmand M, Summers R, Gage FH, Anderson AJ. Human neural stem cells differentiate and promote locomotor recovery in spinal cord-injured mice. Proc Natl Acad Sci U S A. 2005; 102:14069–74. [PubMed: 16172374]
14. Salazar DL, Uchida N, Hamers FPT, Cummings BJ, Anderson AJ. Human neural stem cells differentiate and promote locomotor recovery in an early chronic spinal cord injury NOD-scid mouse model. PloS One. 2010; 5:e12272. [PubMed: 20806064]
15. Bonner JF, Connors TM, Silverman WF, Kowalski DP, Lemay MA, Fischer I. Grafted neural progenitors integrate and restore synaptic connectivity across the injured spinal cord. J Neurosci. 2011; 31:4675–86. [PubMed: 21430166]
16. Courtine G, Song B, Roy RR, Zhong H, Herrmann JE, Ao Y, Qi J, Edgerton VR, Sofroniew MV. Recovery of supraspinal control of stepping via indirect propriospinal relay connections after spinal cord injury. Nat Med. 2008; 14:69–74. [PubMed: 18157143]
17. Lu P, Wang Y, Graham L, McHale K, Gao M, Wu D, Brock J, Blesch A, Rosenzweig ES, Havton LA, Zheng B, Conner JM, Marsala M, Tuszynski MH. Long-distance growth and connectivity of neural stem cells after severe spinal cord injury. Cell. 2012; 150:1264–73. [PubMed: 22980985]
18. Lu P, Woodruff G, Wang Y, Graham L, Hunt M, Wu D, Boehle E, Ahmad R, Poplawski G, Brock J, Goldstein LSB, Tuszynski MH. Long-distance axonal growth from human induced pluripotent stem cells after spinal cord injury. Neuron. 2014; 83:789–96. [PubMed: 25123310]
19. Kadoya K, Lu P, Nguyen K, Lee-Kubli C, Kumamaru H, Yao L, Knackert J, Poplawski G, Dulin JN, Strobl H, Takashima Y, Biane J, Conner J, Zhang S-C, Tuszynski MH. Spinal cord reconstitution with homologous neural grafts enables robust corticospinal regeneration. Nat Med. 2016; 22:479–87. [PubMed: 27019328]
20. Rosenzweig ES, Brock JH, Culbertson MD, Lu P, Moseanko R, Edgerton VR, Havton LA, Tuszynski MH. Extensive spinal decussation and bilateral termination of cervical corticospinal projections in rhesus monkeys. J Comp Neurol. 2009; 513:151–63. [PubMed: 19125408]
21. Kuypers, HGJM. Anatomy of the descending pathways. In: Brooks, VB.Brookhart, JM., Mountcastle, VB., editors. Handbook of Physiology. Bethesda, MD: The American Physiological Society; 1981. p. 597-666.
22. Lacroix S, Havton LA, McKay H, Yang H, Brant A, Roberts J, Tuszynski MH. Bilateral corticospinal projections arise from each motor cortex in the macaque monkey: a quantitative study. J Comp Neurol. 2004; 473:147–61. [PubMed: 15101086]
23. Galea MP, Darian-Smith I. Manual dexterity and corticospinal connectivity following unilateral section of the cervical spinal cord in the macaque monkey. J Comp Neurol. 1997; 381:307–19. [PubMed: 9133570]
24. Kwon BK, Streijger F, Hill CE, Anderson AJ, Bacon M, Beattie MS, Blesch A, Bradbury EJ, Brown A, Bresnahan JC, Case CC, Colburn RW, David S, Fawcett JW, Ferguson AR, Fischer I, Floyd CL, Gensel JC, Houle JD, Jakeman LB, Jeffery ND, Jones LAT, Kleitman N, Kocsis J, Lu P, Magnuson DSK, Marsala M, Moore SW, Mothe AJ, Oudega M, Plant GW, Rabchevsky AS, Schwab JM, Silver J, Steward O, Xu X-M, Guest JD, Tetzlaff W. Large animal and primate models of spinal cord injury for the testing of novel therapies. Exp Neurol. 2015; 269:154–68. [PubMed: 25902036]
25. Tuszynski, MH. Translational Neuroscience: Conclusion. In: Tuszynski, MH., editor. Translational Neuroscience. Springer US; 2016. p. 581-4.
26. Anderson AJ, Piltti KM, Hooshmand MJ, Nishi RA, Cummings BJ. Preclinical Efficacy Failure of Human CNS-Derived Stem Cells for Use in the Pathway Study of Cervical Spinal Cord Injury. Stem Cell Rep. 2017; 8:249–63.

27. Rosenzweig ES, Courtine G, Jindrich DL, Brock JH, Ferguson AR, Strand SC, Nout YS, Roy RR, Miller DM, Beattie MS, Havton LA, Bresnahan JC, Edgerton VR, Tuszynski MH. Extensive spontaneous plasticity of corticospinal projections after primate spinal cord injury. Nat Neurosci. 2010; 13:1505–10. [PubMed: 21076427]

28. Cizkova D, Kakinohana O, Kucharova K, Marsala S, Johe K, Hazel T, Hefferan MP, Marsala M. Functional recovery in rats with ischemic paraplegia after spinal grafting of human spinal stem cells. Neuroscience. 2007; 147:546–60. [PubMed: 17524565]

29. Guo X, Johe K, Molnar P, Davis H, Hickman J. Characterization of a human fetal spinal cord stem cell line, NSI-566RSC, and its induction to functional motoneurons. J Tissue Eng Regen Med. 2010; 4:181–93. [PubMed: 19950213]

30. Glass JD, Boulis NM, Johe K, Rutkove SB, Federici T, Polak M, Kelly C, Feldman EL. Lumbar intraspinal injection of neural stem cells in patients with amyotrophic lateral sclerosis: results of a phase I trial in 12 patients. Stem Cells. 2012; 30:1144–51. [PubMed: 22415942]

31. Sun W, Cornwell A, Li J, Peng S, Osorio MJ, Aalling N, Wang S, Benraiss A, Lou N, Goldman SA, Nedergaard M. SOX9 Is an Astrocyte-Specific Nuclear Marker in the Adult Brain Outside the Neurogenic Regions. J Neurosci. 2017; 37:4493–507. [PubMed: 28336567]

32. Ren Y, Ao Y, O'Shea TM, Burda JE, Bernstein AM, Brumm AJ, Muthusamy N, Ghashghaei HT, Carmichael ST, Cheng L, Sofroniew MV. Ependymal cell contribution to scar formation after spinal cord injury is minimal, local and dependent on direct ependymal injury. Sci Rep. 2017; 7:41122. [PubMed: 28117356]

33. Golan N, Adamsky K, Kartvelishvily E, Brockschnieder D, Möbius W, Spiegel I, Roth AD, Thomson CE, Rechavi G, Peles E. Identification of Tmem10/Opalin as an oligodendrocyte enriched gene using expression profiling combined with genetic cell ablation. Glia. 2008; 56:1176–86. [PubMed: 18571792]

34. Lu P, Ceto S, Wang Y, Graham L, Wu D, Kumamaru H, Staufenberg E, Tuszynski MH. Prolonged human neural stem cell maturation supports recovery in injured rodent CNS. J Clin Invest. 2017; 127:3287–99. [PubMed: 28825600]

35. Greig LC, Woodworth MB, Galazo MJ, Padmanabhan H, Macklis JD. Molecular logic of neocortical projection neuron specification, development and diversity. Nat Rev Neurosci. 2013; 14:755–69. [PubMed: 24105342]

36. Fields HL, Heinricher MM, Mason P. Neurotransmitters in nociceptive modulatory circuits. Annu Rev Neurosci. 1991; 14:219–45. [PubMed: 1674413]

37. Schmidt BJ, Jordan LM. The role of serotonin in reflex modulation and locomotor rhythm production in the mammalian spinal cord. Brain Res Bull. 2000; 53:689–710. [PubMed: 11165804]

38. Nout YS, Ferguson AR, Strand SC, Moseanko R, Hawbecker S, Zdunowski S, Nielson JL, Roy RR, Zhong H, Rosenzweig ES, Brock JH, Courtine G, Edgerton VR, Tuszynski MH, Beattie MS, Bresnahan JC. Methods for functional assessment after C7 spinal cord hemisection in the rhesus monkey. Neurorehabil Neural Repair. 2012; 26:556–69. [PubMed: 22331214]

39. Nout YS, Rosenzweig ES, Brock JH, Strand SC, Moseanko R, Hawbecker S, Zdunowski S, Nielson JL, Roy RR, Courtine G, Ferguson AR, Edgerton VR, Beattie MS, Bresnahan JC, Tuszynski MH. Animal models of neurologic disorders: a nonhuman primate model of spinal cord injury. Neurotherapeutics. 2012; 9:380–92. [PubMed: 22427157]

40. Salegio EA, Bresnahan JC, Sparrey CJ, Camisa W, Fischer J, Leasure J, Buckley J, Nout-Lomas YS, Rosenzweig ES, Moseanko R, Strand S, Hawbecker S, Lemoy M-J, Haefeli J, Ma X, Nielson JL, Edgerton VR, Ferguson AR, Tuszynski MH, Beattie MS. A Unilateral Cervical Spinal Cord Contusion Injury Model in Non-Human Primates (Macaca mulatta). J Neurotrauma. 2016; 33:439–59. [PubMed: 26788611]

41. Friedli L, Rosenzweig ES, Barraud Q, Schubert M, Dominici N, Awai L, Nielson JL, Musienko P, Nout-Lomas Y, Zhong H, Zdunowski S, Roy RR, Strand SC, van den Brand R, Havton LA, Beattie MS, Bresnahan JC, Bézard E, Bloch J, Edgerton VR, Ferguson AR, Curt A, Tuszynski MH, Courtine G. Pronounced species divergence in corticospinal tract reorganization and functional recovery after lateralized spinal cord injury favors primates. Sci Transl Med. 2015; 7:302ra134.

42. Windrem MS, Nunes MC, Rashbaum WK, Schwartz TH, Goodman RA, McKhann G, Roy NS, Goldman SA. Fetal and adult human oligodendrocyte progenitor cell isolates myelinate the congenitally dysmyelinated brain. Nat Med. 2004; 10:93–7. [PubMed: 14702638]
43. Osorio MJ, Goldman SA. Glial progenitor cell-based treatment of the childhood leukodystrophies. Exp Neurol. 2016; 283:476–88. [PubMed: 27170209]
44. Steward O, Sharp KG, Yee KM, Hatch MN, Bonner JF. Characterization of ectopic colonies that form in widespread areas of the nervous system with neural stem cell transplants into the site of a severe spinal cord injury. J Neurosci. 2014; 34:14013–21. [PubMed: 25319698]
45. Tuszynski MH, Wang Y, Graham L, Gao M, Wu D, Brock J, Blesch A, Rosenzweig ES, Havton LA, Zheng B, Conner JM, Marsala M, Lu P. Neural stem cell dissemination after grafting to CNS injury sites. Cell. 2014; 156:388–9. [PubMed: 24485445]
46. Mongiat LA, Espósito MS, Lombardi G, Schinder AF. Reliable Activation of Immature Neurons in the Adult Hippocampus. PLOS ONE. 2009; 4:e5320. [PubMed: 19399173]
47. Dieni CV, Panichi R, Aimone JB, Kuo CT, Wadiche JI, Overstreet-Wadiche L. Low excitatory innervation balances high intrinsic excitability of immature dentate neurons. Nat Commun. 2016; 7:11313. [PubMed: 27095423]
48. Hollis ER, Jamshidi P, Löw K, Blesch A, Tuszynski MH. Induction of corticospinal regeneration by lentiviral trkB-induced Erk activation. Proc Natl Acad Sci U S A. 2009; 106:7215–20. [PubMed: 19359495]
49. Ghosh M, Tuesta LM, Puentes R, Patel S, Melendez K, El Maarouf A, Rutishauser U, Pearse DD. Extensive cell migration, axon regeneration, and improved function with polysialic acid-modified Schwann cells after spinal cord injury. Glia. 2012; 60:979–92. [PubMed: 22460918]
50. Liu K, Lu Y, Lee JK, Samara R, Willenberg R, Sears-Kraxberger I, Tedeschi A, Park KK, Jin D, Cai B, Xu B, Connolly L, Steward O, Zheng B, He Z. PTEN deletion enhances the regenerative ability of adult corticospinal neurons. Nat Neurosci. 2010; 13:1075–81. [PubMed: 20694004]
51. Jin D, Liu Y, Sun F, Wang X, Liu X, He Z. Restoration of skilled locomotion by sprouting corticospinal axons induced by co-deletion of PTEN and SOCS3. Nat Commun. 2015; 6:8074. [PubMed: 26598325]
52. Tuszynski MH, Gabriel K, Gerhardt K, Szollar S. Human spinal cord retains substantial structural mass in chronic stages after injury. J Neurotrauma. 1999; 16:523–31. [PubMed: 10391368]
53. Lu, P., Ahmad, R., Tuszynski, MH. Neural Stem Cells for Spinal Cord Injury. In: Tuszynski, MH., editor. Translational Neuroscience. Springer US; 2016. p. 297-315.
54. Christie KJ, Webber CA, Martinez JA, Singh B, Zochodne DW. PTEN Inhibition to Facilitate Intrinsic Regenerative Outgrowth of Adult Peripheral Axons. J Neurosci. 2010; 30:9306–15. [PubMed: 20610765]
55. Schmid AC, Byrne RD, Vilar R, Woscholski R. Bisperoxovanadium compounds are potent PTEN inhibitors. FEBS Lett. 2004; 566:35–8. [PubMed: 15147864]
56. Raff MC, Barres BA, Burne JF, Coles HS, Ishizaki Y, Jacobson MD. Programmed cell death and the control of cell survival: lessons from the nervous system. Science. 1993; 262:695–700. [PubMed: 8235590]
57. Raff MC. Size control: the regulation of cell numbers in animal development. Cell. 1996; 86:173–5. [PubMed: 8706120]
58. Jacobson MD, Weil M, Raff MC. Programmed cell death in animal development. Cell. 1997; 88:347–54. [PubMed: 9039261]
59. Maor-Nof M, Yaron A. Neurite pruning and neuronal cell death: spatial regulation of shared destruction programs. Curr Opin Neurobiol. 2013; 23:990–6. [PubMed: 23871216]
60. Kaiser HF. Directional statistical decisions. Psychol Rev. 1960; 67:160–7. [PubMed: 14404042]
61. Cattell RB. The Scree Test For The Number Of Factors. Multivar Behav Res. 1966; 1:245–76.
62. Guadagnoli E, Velicer WF. Relation of sample size to the stability of component patterns. Psychol Bull. 1988; 103:265–75. [PubMed: 3363047]
63. Ferguson AR, Irvine K-A, Gensel JC, Nielson JL, Lin A, Ly J, Segal MR, Ratan RR, Bresnahan JC, Beattie MS. Derivation of multivariate syndromic outcome metrics for consistent testing across multiple models of cervical spinal cord injury in rats. PloS One. 2013; 8:e59712. [PubMed: 23544088]

64. Little, RJA., Rubin, DB. Statistical analysis with missing data. 2. New York: John Wiley & Sons, Inc; 2002.

65. Bacchetti P, Deeks SG, McCune JM. Breaking free of sample size dogma to perform innovative translational research. Sci Transl Med. 2011; 3:87ps24.

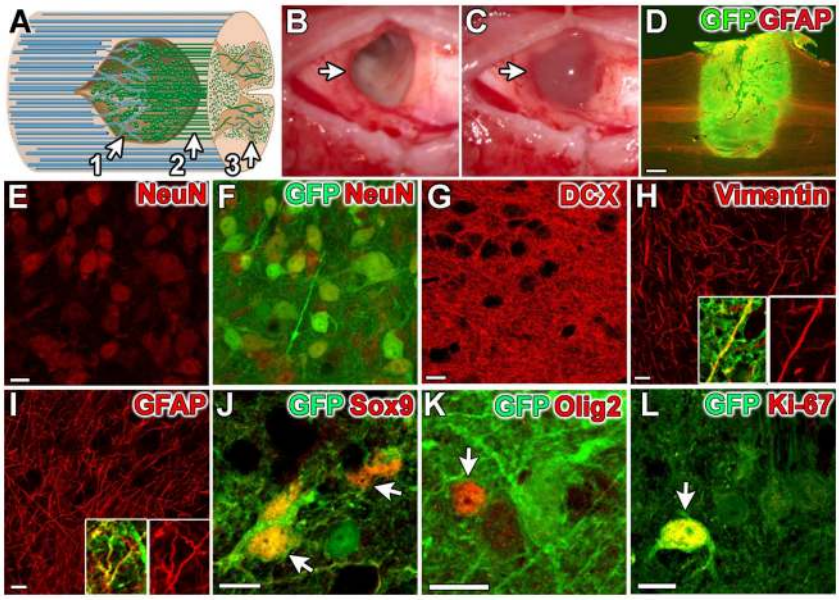

Figure 1. Graft Concept, Procedure, Survival, And Differentiation

(A) Schematic of neural stem cell grafting and functional relay forma tion across a contusion injury site (brown). Host axons (blue) grow into the graft (1), graft axons (green) grow into the host spinal cord (2) to complete the relay circuit (3). (**B**) Surface of spinal cord, with dura retracted laterally and lesion cavity visible (arrow). (**C**) After grafting, the slightly opaque suspension of hNPCs in the fibrin matrix is visible in the lesion site (arrow). (**D**) Human spinal cord neural progenitor cell graft (GFP^+) is well-integrated into a rhesus monkey C7 hemisection lesion site. Horizontal section, rostral to the left. (**E–F**) NeuN alone and merged GFP image in 5-month graft. (**G**) Doublecortin (early neuronal marker) and (**H**) vimentin (early glial marker) were present in all grafts. (**I**) GFAP (mature astrocyte marker) was only present in 5- and 9-month grafts (5 month graft shown). Vimentin and GFAP insets shown with and without GFP. (**J**) Sox9 (astrocyte and ependymal cell marker) was present in all grafts (arrows); at 5 and 9 months, 80% of these cells were astrocytes ($GFAP^+$). (**K**) Olig2 (oligodendrocyte precursor and immature oligodendrocyte marker) was present in all grafts (arrow) (**L**) Ki-67 (dividing cell marker) observed at low (1.5%) but detectable levels (arrow) at all time points. Scale bars: D, 1 mm; E–L, 10 μm. Panels E–F consist of five 0.5 μm confocal optical planes, Panels G, J, K, and L consist of two 0.5 μm confocal optical planes, and Panels H and I are single 0.5 μm confocal optical planes.

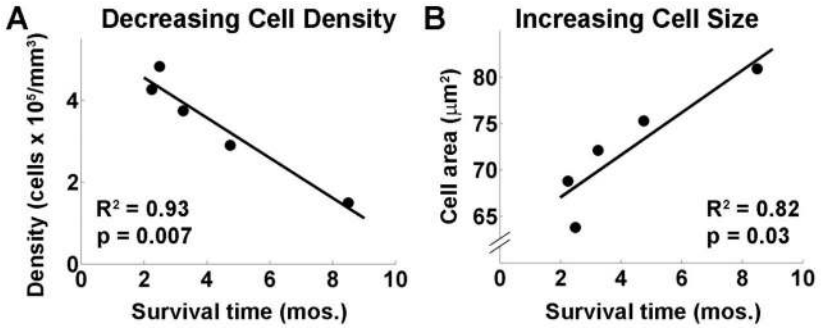

Figure 2. Changes in Graft Density and Cell Size

(**A**) Graft cell density significantly declined over time (P = 0.007, N=5 animals, Matlab corrcoef). (**B**) Mean cell size increased (P = 0.03, N=5 animals, Matlab corrcoef).

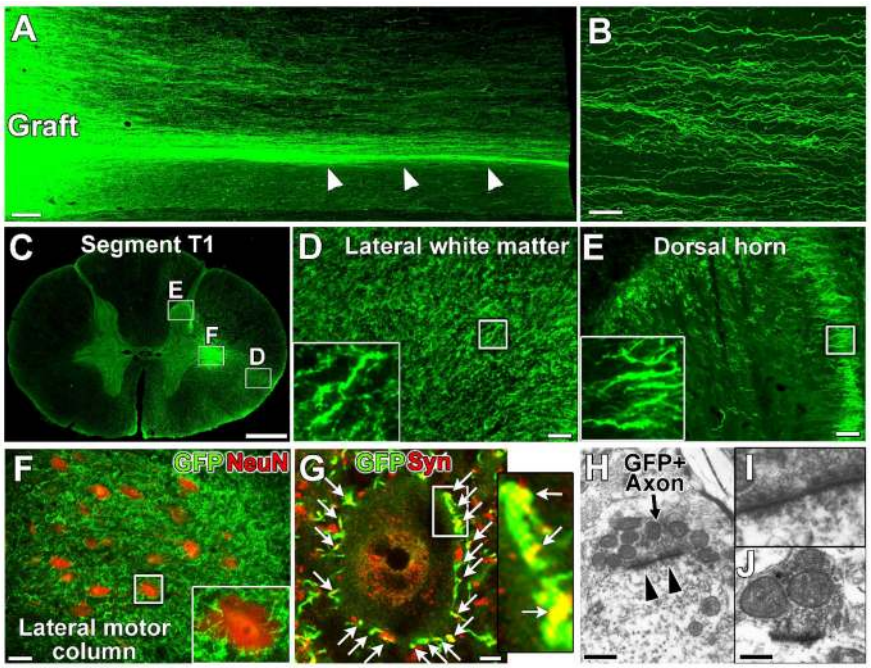

Figure 3. Axon Emergence from Grafts

(A) Large numbers of human, GFP-expressing axons emerge from lesion/graft site and grow caudally in linear arrays. Many axons travel at host white/gray matter interface (arrowheads). Horizontal section, subject 5. **(B)** Numerous linear axons present in host white matter 6mm caudal to the lesion site. **(C)** Large numbers of axons extend into spinal cord segment T1, 7mm caudal to the lesion. **(D–F)** Coronal sections at T1 demonstrating high density of human NSC-derived axons in **(D)** lateral white matter, **(E)** superficial laminae of the dorsal horn, and **(F)** lateral motor neuron column, densely surrounding ventral motor neurons (inset, G). **(G)** Single confocal plane shows many human axon terminals on spinal motor neurons (GFP^+ and $synaptophysin^+$; arrows). **(H–J)** Electron micrographs from T1 ventral gray matter confirm formation of synapses (arrowheads) between GFP^+ human axons and host dendrites. Asymmetric synaptic morphology and circular, dense-core vesicles suggest an excitatory synapse. Panel I is a higher magnification of Panel H; Panel J is a second example. Scale bars: A, 250 μm; B, 20 μm; C, 1 mm; D,E,F, 50 μm; G, 10 μm; H, 250 nm; J, 100 nm.

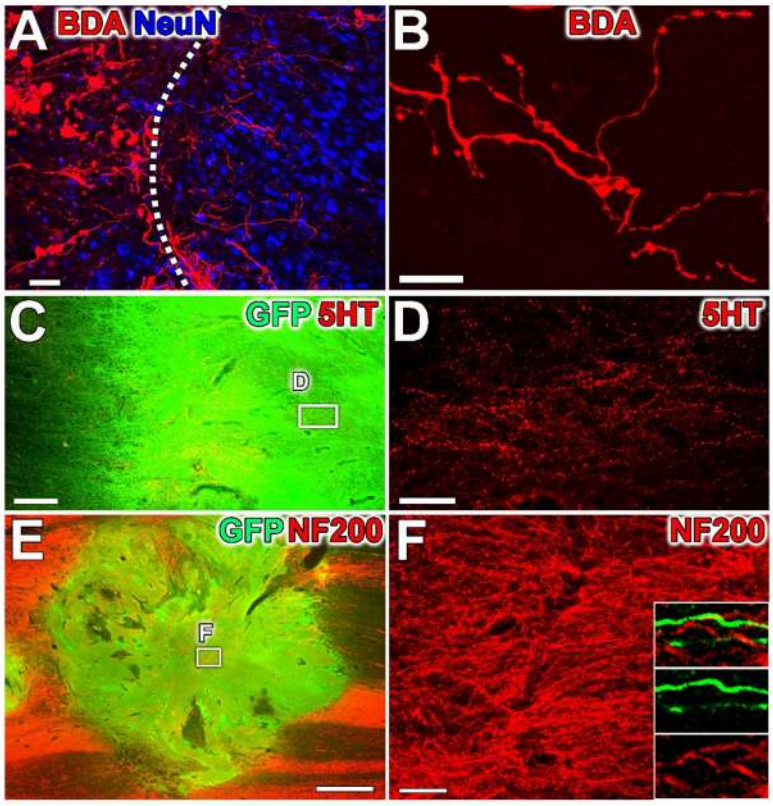

Fig. 4. Host Axons Regenerate into Human NPC Grafts

(A) Corticospinal axons (BDA) regenerate short distances (up to 500 μm) into human NPC grafts. Dashed line indicates host/graft interface, revealed by NeuN labeling. **(B)** Sample axon 300 μm within graft, with complex branching pattern and bouton-like swellings. **(C–D)** Serotonergic (5HT) axons regenerate into human NPC grafts in all subjects with good rostral host-graft integration. **(E–F)** Host NF200^{+} axons extensively regenerate into NPC grafts. Insets: Graft-derived GFP^{+} axons do not label for NF200, either within the graft or in host white matter (shown). Scale bars: A,B,D,F, 50 μm; C, 200 μm; E, 1 mm.

Table 1

Individual Subject Data

Millions of cells survived in all grafts. Up to 155,000 axons emerged from grafts, 2mm caudal to lesion site within 3 months of grafting. Axon numbers appeared to be stable from five to nine months.

Subject	Survival time (mos.)	Graft volume (mm3)	Graft density (cells/mm3)	Total cells (millions)	Total axons (2 mm caudal)	Cell size (μm2)
5	2	60.9	426,000	26.0	140,149	68.8
6	3	67.4	374,000	25.0	154,848	72.1
7	2	11.2	483,000	5.4	54,002	63.8
8	5	12.4	290,000	3.6	64,000	75.3
9	9	48.0	149,000	7.0	68,011	80.9